ACADEMIC
World Academic Union

**ISSN** 1746-7659, England, UK
**Journal of Information and Computing Science**
Vol. 15, No. 1, 2020, *pp*.003-015

# Semi analytical solution of MHD asymmetric flow between two porous disks

Vishwanath B. Awati[1] and Manjunath Jyoti
Department of Mathematics, Rani Channamma University, Belagavi-591156, INDIA.
(Received April 02, 2019, accepted May 17, 2019)

**Abstract:** In this paper, we study MHD asymmetric steady incompressible viscous flow of an electrically conducting fluid between two large stationary coaxial porous disks of different permeability in the presence of uniform transverse magnetic field. The governing nonlinear momentum equations in cylindrical co-ordinates together with relevant boundary conditions are reduced to nonlinear ordinary differential equation (NODE) using similarity transformations. The resulting NODE is solved by Computer Extended Series Solution (CESS) and Homotopy Analysis Method (HAM). The analytical solutions are explicitly expressed by recurrence relation for determining the universal coefficients. The nearest singularity is obtained at $R$=4.2981 with help of Domb-Sykes plot which restricts the convergence of the series, using Euler transformation the singularity is mapped to infinity. The obtained solutions are valid for all values of the Reynolds number, magnetic parameter and permeability parameter are presented through graphs and tabular forms to discuss the important features of the flow. The resulting solutions are compared with the earlier literatures which are found to be in good agreement. Further, the region of validity of the series is extended for much larger values of R up to infinity by Pade' approximants.

**Keywords:** MHD; asymmetric flow; CESS; Domb-Sykes plot; Euler transformation; HAM and Pade' approximants.[1]

## 1. Introduction

The analysis of MHD viscous fluid flow between two parallel porous disks is an interesting area of research because of its significant applications in many fields of since and engineering such as hydrodynamical machines and apparatus, magnetic storage devices, thermal power generating systems, medical equipments, rotating machinery, computer storage devices, gas turbine engines, air cleaning machines, crystal growth processes, geothermal, oceanography, geophysical, biomechanics, design of thrust bearings and most importantly aerodynamic applications etc. Siddique *et al.* [1] and Khan *et al.* [2] investigated the flow of a second grade fluid for MHD transient rotation flow and MHD flow between two side walls perpendicular to a plate in a porous medium respectively. Hayat *et al.* [3] discussed the effects of radiation on MHD flow of a Maxwell fluid analytically. Fetecau et al. [4] investigated exact solutions for the helical flow of an Oldroyd-B fluid in a circular cylinder. Ashraf *et al.* [5] studied numerically for the problem of MHD stagnation point flow through a micropolar fluid towards a heated surface. Rudraiah and Chandrasekhara [6] have discussed inner and outer solutions for the MHD flow between parallel porous disks for large suction Reynolds. Rasmussen [7] studied numerically the problem of steady viscous flow between two parallel porous disks. Elcrat [8] discussed the existence and uniqueness of the problem on radial flow of viscous fluid between two coaxial permeable disks. Guar and Chaudhary [9] investigated the effect of heat transfer for laminar flow between parallel disks of different permeability. Phan-Thien and Bush [10] presented an exact solution for the problem of steady viscous flow of a Newtonian fluid between two porous disks. Rajagopal *et al.* [11-12] discussed the asymmetric flow above a rotating disk and also obtained the numerical solution for the asymmetric flow between parallel rotating disks for a set of values of the governing parameters. Singh *et al.* [13] investigated the experimental and numerical results to discuss the effect of acceleration on flow field. Attia [14] analyzed the effectiveness of the ion slip on the steady flow of an incompressible viscous electrically conducting fluid due to a porous rotating disk with heat transfer. Ersoy [15] examined an approximate solution for the viscous fluid flow between disks rotating about distinct vertical axes for different speeds to study the dependence of velocity fields on the position, the Reynolds number, the eccentricity, and the ratio of angular speeds of the disks. Fang and Zhang [16]

[1] Corresponding Author *E-mail*: awati_vb@yahoo.com.

find an exact solution for the problem of an axisymmetric flow over a stretchable disk by neglecting the body forces and also discussed the effects of disk stretching and stretching Reynolds number with the help of Von Karman's similarity transformations. Bhatt and Hamza [17] presented the similarity solution for the squeezed film flow between two rotating naturally permeable disks.

In this paper, we present the series solutions for the MHD asymmetric flow between porous disks of different permeability in the presence of transverse magnetic field. We obtain the solution for small as well as large Reynolds number using CESS and HAM where as previous authors [18] presented the solutions based on finite difference method for small Reynolds number. In the first method, we investigate the flow problem using CESS based on regular perturbation method. In CESS method, we first calculate sufficiently large number terms of the low Reynolds number perturbation series by using Mathematica so that the nature and location of the singularity can be predicted quite accurately by using Domb-Sykes plot. Secondly, the analytic continuation is used effectively for extending the validity of the perturbation series to moderately higher Reynolds number. Euler transformation is used for the analysis and improvement of the series. Further, we use Pade approximants for summing the Eulerised series to extend the validity of the series for large value of Reynolds number up to infinity. The salient features of this method are evidently explained by Van Dyke [19]. Bujurke and his associates [20-23] have clearly shown the potential applications of these methods in computational fluid dynamics.

We also investigate the same flow problem using fast converging semi-analytical method called Homotopy analysis method (HAM) proposed by Liao [24]. The HAM provides us with a convenient way to control and adjust the convergence region and rate of approximating the solution by series. In this method we have the liberty to choose base functions of the required solution and the corresponding auxiliary linear operator. Therefore, the HAM has great features and advantages over all other analytical approximate methods, so it is also easy to use for the physical problems arises in flow problems. Recently, Awati et al. [25] studied the solution of MHD flow of viscous fluid between parallel porous plates in the presence of the magnetic field using CESS and HAM.

The paper is outlined as follows. Section 1 is devoted to describe the introduction; section 2 develops the mathematical formulation of the proposed problem with relevant boundary conditions. The solution of the problem is obtained by Computer extended series and Homotopy analysis method in section 3 and 4 respectively. Section 5 presents results and discussion; section 6 is about the conclusion.

## 2. Mathematical Formulation

Let us consider the MHD asymmetric steady incompressible viscous flow of an electrically conducting fluid between two stationary coaxial porous disks of infinite radii coinciding with the planes z = $\pm a$ with constant injection velocities $V_1$ and $V_2$ at the lower and upper disks respectively in the presence of a uniform transverse magnetic field of intensity $B_0$.The geometry of the governing physical flow problem is shown in Fig. 1.

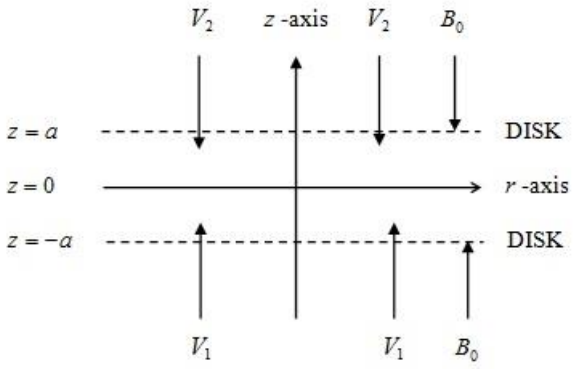


Fig.1 Geometry of the physical phenomenon.

In order to investigate the effects of different permeability of the disks it's necessary to define the following permeability parameter as fallows

$$A = 1 - \frac{V_1}{V_2} \tag{2.1}$$

The velocity components *u*, *v*, *w* along radial, transverse and axial directions respectively for the present problems are

$$u = u(r,z), v = 0, w = w(r,z) \tag{2.2}$$

The governing continuity and momentum equations in cylindrical coordinate system for an electrically conducting incompressible fluid in the presence of uniform magnetic field are given by

$$\frac{\partial u}{\partial r} + \frac{u}{r} + \frac{1}{a}\frac{\partial w}{\partial \eta} = 0\,, \tag{2.3}$$

$$\rho\left(u\frac{\partial u}{\partial r} + \frac{w}{a}\frac{\partial u}{\partial \eta}\right) = -\frac{\partial p}{\partial r} + \mu\left(\frac{\partial^2 u}{\partial r^2} + \frac{1}{r}\frac{\partial u}{\partial r} - \frac{u}{r^2} + \frac{1}{a^2}\frac{\partial^2 u}{\partial \eta^2}\right) - \sigma_e B_0^2 u, \tag{2.4}$$

$$\rho\left(u\frac{\partial w}{\partial r} + \frac{w}{a}\frac{\partial w}{\partial \eta}\right) = -\frac{1}{a}\frac{\partial p}{\partial \eta} + \mu\left(\frac{\partial^2 w}{\partial r^2} + \frac{1}{r}\frac{\partial w}{\partial r} + \frac{1}{a^2}\frac{\partial^2 w}{\partial \eta^2}\right), \tag{2.5}$$

where $\mu$ is the viscosity of the fluid, $p$ be the pressure of the fluid and $\rho$ is the density of the fluid, $\sigma_e$ be the electrical conductivity and $B_0$ be the magnetic field intensity. The corresponding boundary conditions for the velocity field at the two porous disks are

$$u(r,-1) = 0, u(r,+1) = 0, w(r,-1) = V_1, w(r,+1) = V_2. \tag{2.6}$$

where $V_1$ and $V_2$ are uniform velocities at the lower and upper disks respectively. Introducing the dimensionless similarity variables $f$ and $\eta$ as fallows

$$\psi(r,\eta) = \frac{V_2 r^2}{2} f(\eta) and \eta = \frac{z}{a} \tag{2.7}$$

The velocity components u and w are related to the physical stream function $\psi(r,\eta)$ and these are similar to that of Von Karman [26] and Elkouh [27] such as

$$u = \frac{1}{ra}\frac{\partial \psi}{\partial \eta} = \frac{V_2 r}{2a} f'(\eta) \tag{2.8}$$

$$w = -\frac{1}{r}\frac{\partial \psi}{\partial r} = -V_2 f(\eta) \tag{2.9}$$

The above velocity fields are satisfies the continuity equation (2.3) automatically. Substituting the Eqns. (2.8-2.9) in momentum equations (2.4-2.5), after eliminating the pressure term we get

$$f'''' + R(ff''' - M^2 f'') = 0 \tag{2.10}$$

where $R = \frac{\rho V_2 a}{\mu}$ is the Reynolds number and $M = \sqrt{\frac{\sigma_e a B_0^2}{\rho V_2}}$ is the Hartmann number.

The reduced boundary conditions of the governing problem are

$$f(-1) = 1 - A, f(1) = 1, f'(-1) = 0, f'(1) = 0 \tag{2.11}$$

## 3. Series solution

We employ a regular perturbation method for the solution of Eqn. (2.10) in powers of R in the form

$$f(\eta) = \sum_{n=0}^{\infty} R^n f_n(\eta) \tag{3.12}$$

Substituting Eqn. (3.14) into Eqn. (2.11) and equating like powers of *R* on both sides, we get

$$f_0'''' = 0 \tag{3.13}$$

$$f_{n+1}'''' = -f_0 f_n''' - f_n f_0''' - \sum_{L=1}^{n-1}[f_L f_m'''] + M^2 f_n'', \qquad n = 1,2,3 \ldots\ldots \tag{3.14}$$

where $m = n - L$. The associated boundary conditions are

$$f_0(-1) = 1 - A, f_0(1) = 1, f_0'(-1) = 0, f_0'(1) = 0, \tag{3.15}$$

$$f_n(-1) = 0, f_n(1) = 0, f_n'(-1) = 0, f_n'(1) = 0, \qquad n \geq 1 \tag{3.16}$$

The solutions of the above equations satisfying the boundary conditions are given by

$f_0 = \frac{1}{4}(4 - 2A) + \frac{3A}{4}\eta - \frac{A}{4}\eta^3$

$$f_1 = \frac{A}{16} - \frac{A^2}{32} + \left(\frac{19A^2}{2240} - \frac{AM^2}{80}\right)\eta + \left(-\frac{A}{8} + \frac{A^2}{16}\right)\eta^2 + \left(-\frac{39A^2}{2240} - \frac{AM^2}{40}\right)\eta^3 + \left(-\frac{A}{16} + \frac{A^2}{32}\right)\eta^4 \tag{3.17}$$

$$+ \left(-\frac{3A^2}{320} - \frac{AM^2}{80}\right)\eta^5 - \frac{A^2}{2240}\eta^7$$

$$f_2 = -\frac{31A^2}{26880}+\frac{31A^3}{53760}-\frac{AM^2}{120}+\frac{A^2M^2}{240}+\left(-\frac{A}{80}+\frac{A^2}{80}-\frac{177A^3}{53900}-\frac{A^2M^2}{4480}+\frac{11AM^4}{16800}\right)\eta$$
$$+\left(-\frac{A^2}{448}+\frac{A^3}{896}+\frac{AM^2}{48}-\frac{A^2M^2}{96}\right)\eta^2+\left(\frac{A}{40}-\frac{A^2}{40}+\frac{25429A^3}{4139520}+\frac{43A^2M^2}{33600}-\frac{9AM^4}{5600}\right)\eta^3$$
$$+\left(\frac{37A^2}{4480}-\frac{37A^3}{8960}-\frac{AM^2}{60}+\frac{A^2M^2}{120}\right)\eta^4+\left(-\frac{A}{80}+\frac{A^2}{80}-\frac{53A^3}{22400}-\frac{11A^2M^2}{5600}+\frac{AM^4}{800}\right)\eta^5$$
$$+\left(-\frac{A^2}{192}+\frac{A^3}{384}+\frac{AM^2}{240}-\frac{A^2M^2}{480}\right)\eta^6+\left(-\frac{177A^3}{313600}+\frac{11A^2M^2}{11200}-\frac{AM^4}{3360}\right)\eta^7+\left(\frac{3A^2}{8960}-\frac{3A^3}{17920}\right)\eta^8$$
$$+\left(\frac{A^3}{13440}-\frac{A^2M^2}{13440}\right)\eta^9-\frac{3A^3}{985600}\eta^{11}$$

### 3.1 Computer extended series

We cannot analyze the important features of the flow problem just by using the above three approximations of the series. It is necessary to generate the large number of terms (universal polynomial coefficients) to analyze the series which reveal the true nature of the solution representing the physical problem. As we proceed for calculating the higher order terms, the algebra becomes tedious thus it is difficult to calculate the higher terms manually but it can be made automatically using Mathematica. Based on the nature of solution functions (3.17), we propose a general form $f_n(\eta)$ to be of the form

$$f_n(\eta) = \sum_{k=4}^{4n+3} A_{(n,k)}[\eta^{(k-4)} - 2\eta^{(k-2)} + \eta^k], n = 1,2,3, \ldots\ldots \tag{3.18}$$

The above expression generates exactly the earlier obtained solutions $f_i$ for $(i = 1,2)$. Using the following recurrence relation and Mathematica we can generate $f_i$ for $(i > 2)$. Substitute Eqn. (3.18) into Eqn. (3.14) and equate various powers of $\eta$ on both sides and obtain a recurrence formula for generating the unknown universal coefficients $A_{(n,k)}$ in the form

$$A_{(n+1,4n-(2J+1))} = 2A_{(n+1,4n-(2J-1))} - A_{(n+1,4n-(2J-3))} +$$
$$\frac{1}{(4n-(2J+1))(4n-(2J+2))(4n-(2J+3))(4n-(2J+4))}$$
$$\times\left\{A_{(n+1,4n-(2J+5))}S_1(k) + \sum_{i=2}^{7} A_{(n,+1,4n-(2J+5)+i)}S_i(4n-(2J+5)+i)\right.$$
$$\left.-\sum_{L=1}^{n-1}\left[\sum_{r=-2}^{2}\left(\sum_{k_1=4L-(2J+1)-2r}^{4L+3} A_{(L,k_1)}\cdot A_{(m,4n-k_1-(2J-2)-2r)}\, S_{10-r}(k_1, 4n-k_1-(2J-2)-2r)\right)\right]\right\} \tag{3.19}$$

where $m = n - L$ and $J$ varies form $-4,-3,-2,-1,0,1,\ldots\ldots(2n-2)$.

$$S_1(k) = \frac{A}{4}k(k-1)(k-2)+\frac{3A}{2},$$

$$S_2(k) = M^2k(-1) - 3A - \frac{A}{2}(k-2)(k-3)(k-4) - \frac{3A}{4}k(k-1)(k-2),$$

$$S_3(k) = (-1+\frac{1}{2}A)k(k-1)(k-2),$$

$$S_4(k) = \frac{3A}{2}(k-2)(k-3)(k-4)+\frac{A}{4}(k-4)(k-5)(k-6)+\frac{3A}{2}-2M^2(k-2)(k-3)$$

$$S_5(k) = \left(1-\frac{1}{2}A\right)2(k-2)(k-3)(k-4),$$

$$S_6(k) = M^2(k-4)(k-5) - \frac{3A}{4}(k-4)(k-5)(k-6),$$

$$S_7(k) = \left(-1+\frac{1}{2}A\right)(k-4)(k-5)(k-6),$$

$$S_8(k_1,k_2) = k_2(k_2-1)(k_2-2),$$

$$S_8(k_1,k_2) = -2k_2(k_2-1)(k_2-2) - 2(k_2-2)(k_2-3)(k_2-4),$$

$S_{10}(k_1,k_2) = k_2(k_2-1)(k_2-2) + 4(k_2-2)(k_2-3)(k_2-4) + (k_2-4)(k_2-5)(k_2-6),$

$S_{11}(k_1,k_2) = -2(k_2-2)(k_2-3)(k_2-4) - 2(k_2-4)(k_2-5)(k_2-6),$

$S_{12}(k_1,k_2) = (k_2-4)(k_2-5)(k_2-6).$

The expression for axial velocity profile at the porous disks in the form

$$f(\eta) = \frac{1}{4}(4-2A) + \frac{3A}{4}\eta - \frac{A}{4}\eta^3 + \sum_{n=1}^{\infty} R^n \sum_{k=4}^{4n+3} A_{(n,k)}[\eta^{(k-4)} - 2\eta^{(k-2)} + \eta^k]. \quad (3.20)$$

The shear stress on the lower disk is given by

$$f''(-1) = \frac{3A}{2} + \sum_{n=1}^{\infty} C_{n+1} R^n \quad (3.21)$$

where $C_{n+1} = \sum_{k=4}^{4n+3} 12A_{(n,k)}$.

## 3.2 Analysis and improvement of the series

The universal polynomial coefficients of the series (3.21) representing shear stress at the lower disk have alternative signs and decreases in magnitude. These coefficients indicate the presence of nearest singularity lying on the negative y-axis ($R$=-$R_0$) has no direct physical significance. Using the computed coefficients in the series (3.21) we draw the Domb-Sykes plot [28] for $A$=1.4 and $M$=1.2 as shown in Fig.2. Results are further extrapolated using rational approximation [29] for finding quite accurate values of radii of convergence of the series (3.21) to be $R_0$=4.2981. The direct sums of the series for axial and radial velocity are valid only up to the radius of the convergence $R_0$. We use Pade' [30] approximants for summing up the series which gives a converging sum for enough larger values of $R$. The series (3.21) is to recast into new form using Euler transformation that helps to improve the region of the validity of the series. With the help of this transformation the singularity is mapped to infinity.

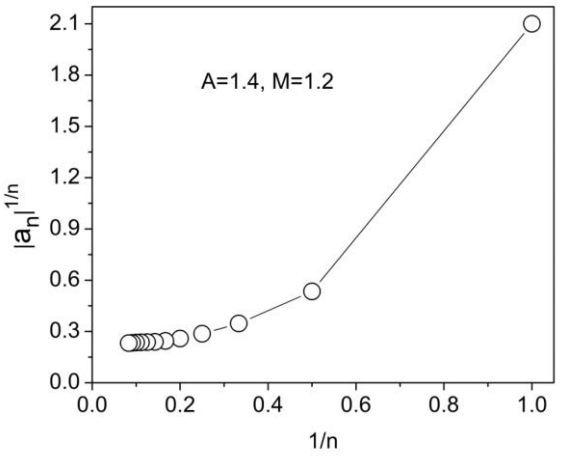


Fig.2 Domb-Sykes plot for the series $f''(-1)$ for $A$=1.4 and $M$=1.2.

## Euler Transformation

The Euler transformation helps in recasting the series into new series whose region of validity is increased compared to the original one. Let the transformation envisages using a new variable $\omega$ such that

$$\omega = \frac{R}{R+R_0} \quad \textbf{Or} \quad R = \frac{\omega R_0}{(1-\omega)}$$

The series (3.21) is recast into new form (Eulerized series)

$$f''(-1) = \frac{3A}{2} + \sum_{n=1}^{\infty} C_{n+1}\left(\frac{\omega R_0}{(1-\omega)}\right)^n = \sum_{n=1}^{\infty} D_n \omega^{n-1} \quad (3.22)$$

where

$D_1 = C_1 = \frac{3A}{2},$

$D_2 = C_2R_0,$

$D_3 = C_2R_0 + C_3R_0^2,$

$D_4 = C_2R_0 + 2C_3R_0^2 + C_4R_0^3,$

$D_5 = C_2R_0 + 3C_3R_0^2 + 3C_4R_0^3 + C_5R_0^4,$

$D_n = (-1)^{n-1}\Delta^{n-2}e_2$,
with
$\Delta e_j = e_{j+1} - e_j$
$e_j = (-R_0)^{j-1}C_j$.
The Eulerized series (3.22) is used to approximate the solution on entire real line, besides this we have used the Pade approximants for summing up the new series which extends the region of the validity of the Reynolds number up to infinity. The results for shear stress based on the series (3.22) are given in Table. 3.

# 4. Homotopy analysis method

We apply HAM for the solution of Eqn. (2.10) subjected to the boundary conditions (2.11). Based on the boundary conditions we select the initial approximation and auxiliary linear operator for the function $f$ as fallows

$$\boldsymbol{f_0(\eta) = \frac{1}{4}(4 - 2A + 3A\eta - A\eta^3)} \tag{4.23}$$

and

$$L[f] = f'''' \tag{4.24}$$

The above linear operator satisfies

$$\boldsymbol{L[C_1\frac{\eta^3}{6} + C_1\frac{\eta^2}{2} + C_3\eta + C_4] = 0} \tag{4.25}$$

in which $C_1, C_2, C_3$ and $C_4$ are arbitrary constants to be determined.

### 4.1 Zeroth-order deformation problem

If $q \in [0,1]$ be the embedding parameter, $\hbar$ is the non-zero auxiliary parameter then the zeroth order deformation problem can be constructed as

$$(1-q)L[f(\eta,q) - f_0(\eta)] = q\hbar\aleph[f(\eta,q)] \tag{4.26}$$

also the boundary conditions becomes

$$f(-1,q) = 1 - A, f(1,q) = 0, f'(-1,q) = 0, f'(1,q) = 0. \tag{4.27}$$

Further $\aleph$ is the non-linear differential operator in the Eqn. (4.26) given by

$$\aleph[f(\eta,q)] = \frac{\partial^4 f(\eta,q)}{\partial\eta^4} + R\left(f(\eta,q)\frac{\partial^3 f(\eta,q)}{\partial\eta^3} - M^2\frac{\partial^2 f(\eta,q)}{\partial\eta^2}\right) \tag{4.28}$$

For $q = 0$ and $q = 1$, Eqn. (4.26) have the solutions respectively as

$$f(\eta,0) = f_0(\eta) \text{ and } f(\eta,1) = f(\eta). \tag{4.29}$$

As $q$ varies from 0 to 1, $f(\eta,q)$ also varies from the initial approximation $f_0(\eta)$ to the exact solution $f(\eta)$. With the help of Taylor's theorem and Eqn. (4.29), it can be written as

$$f(\eta,q) = f_0(\eta) + \sum_{m=1}^{\infty} f_m(\eta)q^m \tag{4.30}$$

where $f_m(\eta) = \frac{1}{m!}\frac{\partial^m f(\eta,q)}{\partial q^m}|_{q=0}$. The convergence of the series (4.30) depends on the auxiliary parameter $\hbar$.To select the value of $\hbar$ in such a way that the series (4.30) is convergent at $q = 1$, then we have

$$f(\eta,q) = f_0(\eta) + \sum_{m=1}^{\infty} f_m(\eta) \tag{4.31}$$

### 4.2 mth-order deformation problem

Differentiating the zeroth order deformation problem (4.26) $'m'$ times with respect to $q$ and then dividing it by $m!$ finally setting $q = 0$. The resulting mth-order deformation problem becomes

$$L[f_m(\eta) - \chi_m f_{m-1}(\eta)] = \hbar\Re_m(\eta) \tag{4.32}$$

and the homogeneous boundary conditions are

$$f_m(-1) = 0, f_m(1) = 0, f_m'(-1) = 0, f_m'(1) = 0, \tag{4.33}$$

where

$$\Re_m(\eta) = f_{m-1}'''' + R\sum_{n=0}^{m-1}[f_n f_{m-1-n}''' - M^2 f_{m-1}''] \tag{4.34}$$

and

$$\chi_m = \begin{cases} 0, m \le 1; \\ 1, m > 1; \end{cases} \tag{4.35}$$

We use Mathematica to solve the linear system of equations (4.32) with the appropriate homogeneous boundary conditions (4.33) up to first few orders of approximations

$$f_1 = \hbar R\left(-\frac{A}{16}+\frac{A^2}{32}+\left(-\frac{19A^2}{2240}+\frac{AM^2}{80}\right)\eta+\left(\frac{A}{8}-\frac{A^2}{16}\right)\eta^2+\left(\frac{39A^2}{2240}-\frac{AM^2}{40}\right)\eta^3+\left(-\frac{A}{16}+\frac{A^2}{32}\right)\eta^4\right.$$
$$\left.+\left(-\frac{3A^2}{320}+\frac{AM^2}{80}\right)\eta^5+\frac{A^2}{2240}\eta^7\right),$$

$$f_2 = -\frac{1}{20697600}A\hbar R(-1+\eta^2)^2(A^2\hbar R(-11935+67968\eta-46970\eta^2+8791\eta^3+3465\eta^4-1414\eta^5+63\eta^7)$$
$$+1232(-210(-5+M^2\eta)+\hbar\left(210(5+R\eta)+M^2R\eta(-11+5\eta^2)-70M^2(3\eta+R(-2+\eta^2))\right))$$
$$+154A(-60(70-19\eta+\eta^3)+\hbar(-60(70-19\eta+\eta^3)+R(5(31-336\eta+122\eta^2-9\eta^4)$$
$$+2M^2\left(-280+15\eta+140\eta^2-56\eta^3+5\eta^5\right))))) \qquad (4.36)$$

## 4.3 Convergence of HAM

The explicit analytic expression (4.31) contains the auxiliary parameter $\hbar$ is called as convergence control parameter, which plays an important role in finding the convergence region and rate of approximation for the HAM solutions.

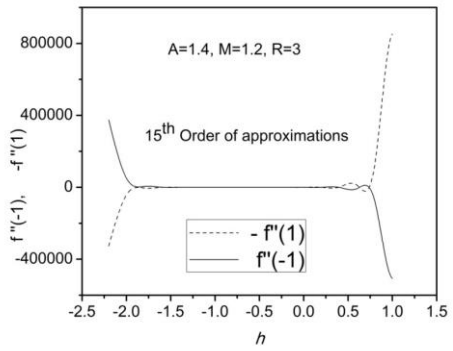


Fig. 3 $\hbar$ curves for the shear stresses for different values of $\gamma$ and *R*.

To predict the permissible ranges of the parameter $\hbar$, we draw the line segments of the $\hbar$ curves parallel to $\eta$ - axis. Fig. 3 shows the $\hbar$ curves for the shear stresses at the lower and upper disks for *A*=1.4, *M*=1.2 and *R*=3 at the 15th order of approximations, it clearly indicates that the admissible ranges of $\hbar$ is$-1.3 \leq \hbar \leq -0.1$. To confirm the admissible range for $\hbar$ we draw $\hbar$ -curve for residual error of $f$ as shown in Fig. 4.

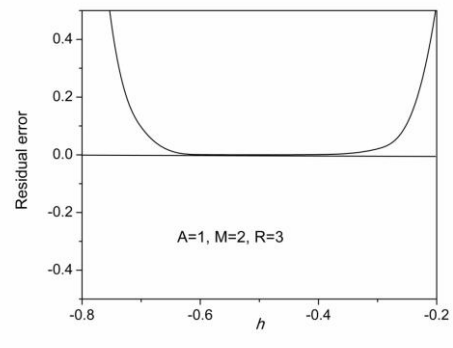


Fig. 4 $\hbar$ curve for the residual error of *f*.

It is also observed that the HAM results are obtained up to four decimal places of accuracy by taking the values of $\hbar$ from this range. Also, our computation depicts that the series converges in the whole region of $-1 \leq \eta \leq 1$ when $\hbar = -0.6$.

## 5. Results and Discussions

The equation of motion for the fluid flow is governed by nonlinear ODE (2.11) together with the boundary conditions (2.10) are solved by using CESS and HAM. A new type of series expansion scheme with universal polynomial coefficients proposed here enables us for obtaining a recurrence formula, which generates large number of universal polynomial coefficients $A_{(n,k)}, k = 4,5,\ldots..4n+3$, these in turn give universal polynomial functions $f_n(\eta)$. The series (3.20) representing velocity profiles which can be improved by using Pade' approximants for much larger values of Reynolds number for various values parameters *A* and *M*. The predictions based on flow behaviors between the porous disks are presented graphically for different parameters in Figs. 5-10. Table 1 presents semi-analytical results of the axial velocities in the whole region of $-1 \leq \eta \leq 1$ and which are compared with earlier numerical values, which shows that the results are in good agreement.

TABLE 1. Dimensionless axial velocity $f(\eta)$ results for *A=1.2, R*=20 and *M* = 0.4.

| | $f(\eta)$ | | |
|---|---|---|---|
| $\eta$ | Numerical | HAM | CESS |
| -1.0 | -0.20000 | -0.20000 | -0.20000 |
| -0.8 | -0.13874 | -0.13873 | -0.13863 |
| -0.6 | 0.01567 | 0.01566 | 0.015498 |
| -0.4 | 0.212503 | 0.212501 | 0.213851 |
| -0.2 | 0.408912 | 0.408909 | 0.409056 |
| 0 | 0.58374 | 0.583739 | 0.584910 |
| 0.2 | 0.730372 | 0.730374 | 0.735998 |
| 0.4 | 0.846612 | 0.846642 | 0.847809 |
| 0.6 | 0.931086 | 0.931066 | 0.931510 |
| 0.8 | 0.982597 | 0.982589 | 0.983745 |
| 1.0 | 1.000016 | 1.000000 | 1.000000 |

The coefficients of the series (3.21) representing shear stress at the lower disk for different values of *A* and *M* have alternative sign patterns and decrease in magnitude. Fig. 2 shows the Domb-Sykes plot, which estimates the location and nature of the nearest singularity restricts the convergence region. The rational extrapolation yields the radius of convergence of the series (3.21) to be $R_0$=4.2981 for the values of *A*=1.4 and *M*=1.2. These universal polynomial coefficients indicates the presence of nearest singularity lying on the negative y-axis ($R$ = -$R_0$) has no direct physical significance. With the help of Euler transformation we recast the old series (3.21) into a new series (Eulerized series) (3.22) which enables in enlarging the region of validity of the series. The Eulerized series (3.22) is the continuation of the series solution analytically to infinity which corresponds to $\omega = 1$ and it is confirmed by the Domb-Sykes plot for the Eulerized series (3.22) as shown in Fig 11. Table 2 shows that the effect of permeability parameter *A* on shear stresses at the lower disk as well as upper disk for the given constant values of suction Reynolds number *R* and Hartmann number *M*. It is observed that an increase in the value of *A*, at the lower disk the magnitudes of the shear stress decreases from its higher value to its lower value while at the upper disk the magnitude of the shear stress increases from its lower value to its higher value. Also it is observed that for the fixed value of *A* = 2, the shear stresses have the same magnitude (value) at the upper and lower disks thus it shows that the symmetry of the problem.

TABLE 2. Shear stresses at the disks for *R=10, M*=0.8 and various values of *A*.

| | $f''(-1)$ | | | $-f''(1)$ | | |
|---|---|---|---|---|---|---|
| *A* | Numerical | HAM | *CESS* | *Numerical* | HAM | CESS |
| 1.0 | 3.2842 | 3.2843 | 3.2811 | 0.9289 | 0.9289 | 0.9362 |
| 1.2 | 3.0954 | 3.0953 | 3.0952 | 1.1821 | 1.1820 | 1.1871 |
| 1.4 | 2.8918 | 2.8918 | 2.8932 | 1.4726 | 1.4725 | 1.4754 |
| 1.6 | 2.7342 | 2.7341 | 2.7336 | 1.8042 | 1.8042 | 1.8055 |
| 1.8 | 2.6378 | 2.6377 | 2.6374 | 2.1781 | 2.1781 | 2.1789 |
| 2.0 | 2.5936 | 2.5936 | 2.5937 | 2.5936 | 2.5936 | 2.5937 |

TABLE 3. Shear stresses at the disks for $A$ = 1.4, $M$ = 1.2 and various values of $R$.

| | $f''(-1)$ | | | $-f''(1)$ | | |
|---|---|---|---|---|---|---|
| *R* | Numerical | HAM | *CESS* | *Numerical* | HAM | CESS |
| 0 | 2.1000 | 2.1000 | 2.1000 | 2.1000 | 2.1000 | 2.1000 |
| 5 | 2.9464 | 2.9464 | 2.9464 | 1.9067 | 1.9067 | 1.9067 |
| 10 | 3.3323 | 3.3324 | 3.3321 | 1.8899 | 1.8899 | 1.8878 |
| 15 | 3.5665 | 3.5666 | 3.5669 | 1.8839 | 1.8839 | 1.8853 |
| 40 | 4.0636 | 4.0635 | 4.0666 | 1.8723 | 1.8723 | 1.8733 |
| 65 | 4.2439 | 4.2439 | 4.2490 | 1.8680 | 1.8686 | 1.8696 |
| 90 | 4.3381 | 4.3363 | 4.3345 | 1.8657 | 1.8656 | 1.8667 |
| 120 | - - - - - - | 4.4063 | 4.4126 | - - - - - - | 1.8643 | 1.8653 |
| 150 | - - - - - - | 4.4496 | 4.4561 | - - - - - - | 1.8632 | 1.8644 |
| 300 | - - - - - - | 4.5439 | 4.5497 | - - - - - - | 1.8604 | 1.8623 |
| 500 | - - - - - - | 4.5846 | 4.5900 | - - - - - - | 1.8593 | 1.8693 |
| 1000 | - - - - - - | 4.6176 | 4.6213 | - - - - - - | 1.8585 | 1.8685 |
| 10000 | - - - - - - | 4.6271 | 4.6504 | - - - - - - | 1.8585 | 1.8685 |

Table 3 demonstrates the influence of Reynolds number $R$ on the shear stresses at both the disks for $A$ = 1.4 & $M$ = 1.2. It is observed that an increase in the value of $R$ at the lower disk the magnitudes of the shear stress increases from its minimum value to its maximum value while at the upper disk the magnitude of the shear stress decreases from its maximum value to its minimum value. It is seen that for $R$ = 0, the shear stresses values are equal at both the disks and thus representing the symmetry of the flow problem. The effect of the Hartmann number $M$ on shear stresses for the constant values of $A$ and $M$ at both the disks are presented in Table 4. It is observed that an increase in the value of $M$ corresponds to gradually increase in the magnitudes of the shear stresses at both the disks.

TABLE 4. Shear stresses at the disks for $A$=*1.2*, $R$=20 and various values of $M$.

| | $f''(-1)$ | | | $-f''(1)$ | | |
|---|---|---|---|---|---|---|
| *M* | Numerical | HAM | *CESS* | *Numerical* | HAM | CESS |
| 0.0 | 3.3069 | 3.3068 | 3.3068 | 0.7999 | 0.7999 | 0.7998 |
| 0.4 | 3.3722 | 3.3722 | 3.3857 | 0.8802 | 0.8802 | 0.8807 |
| 0.8 | 3.6297 | 3.6297 | 3.6204 | 1.1245 | 1.1245 | 1.1249 |
| 1.2 | 4.1361 | 4.1365 | 4.1359 | 1.5297 | 1.5297 | 1.5294 |
| 1.6 | 4.8451 | 4.8456 | 4.8353 | 2.0753 | 2.0753 | 2.0813 |
| 2.0 | 5.6813 | 5.6814 | 5.6650 | 2.7322 | 2.7322 | 2.7352 |
| 2.4 | 6.5921 | 6.5924 | 6.4588 | 3.4736 | 3.4736 | 3.4756 |
| 3.2 | 8.5312 | 8.5329 | 8.4130 | 5.1317 | 5.1317 | 5.1327 |
| 4.0 | 10.5475 | 10.5650 | 10.5173 | 6.9396 | 6.9396 | 6.9316 |
| 6.0 | 15.6995 | 15.6943 | 15.6843 | 11.7792 | 11.7792 | 11.7782 |
| 8.0 | 20.8730 | 20.8725 | 20.8571 | 16.8030 | 16.8030 | 16.8130 |

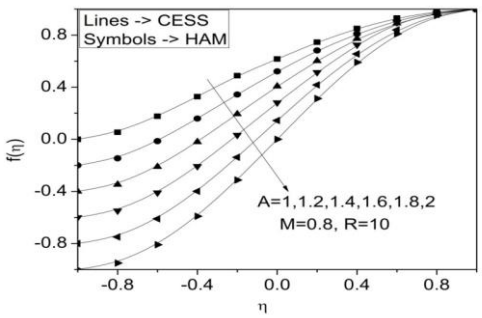


Fig. 5 Variation of axial velocity for $R$=10, $M$=0.8 and various values of $A$.

Figs. 5 and 6 illustrates variations of axial and radial velocity profiles respectively for $R$ = 10 & $M$ = 0.8 for various values of $A$. The axial velocity profiles have drawn between the porous disks for different

permeability parameters in Fig. 5, which are useful in estimating the position of viscous layers developed due to the suction at the two disks. It is observed that by increasing the values of *A*, the position of the viscous layer approaches towards the central plane z = 0 and also the axial velocity profiles values are decreasing for increasing values of *A*. The velocity profiles in the radial direction under different values of *A* are shown in Fig 6. It is seen that the radial velocities are increasing as increase in the values of permeability parameter. Also an interesting fact that the radial velocity shows symmetry for the case *A* = 2 where it gains the maximum velocity.

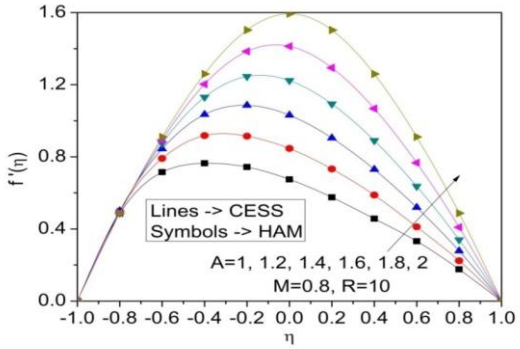


Fig. 6 Variation of radial velocity for *R*=10, *M*=0.8 and various values of *A*.

Fig. 7 describes the effect of Reynolds number *R* (for large R also) on the velocity profiles in the axial direction under constant values of *A &M*. The axial velocity confined its dimensionless value -1 at the lower disk and 1 at the upper disk where the concavity is changed. It is observed that by increasing the values of *R* from 0 to 40, the axial velocity profiles increases significantly. As far as increasing the values of *R* greatly up to infinity, the axial velocities are slightly increasing due to the restrictions of axial velocity on the outer boundaries (are -1 and 1).

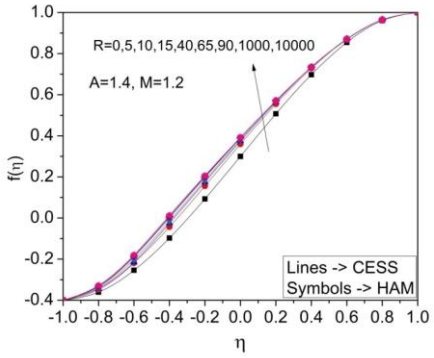


Fig.7 Variation of axial velocity for *A*=1.4, *M*=1.2 and various values of *R*.

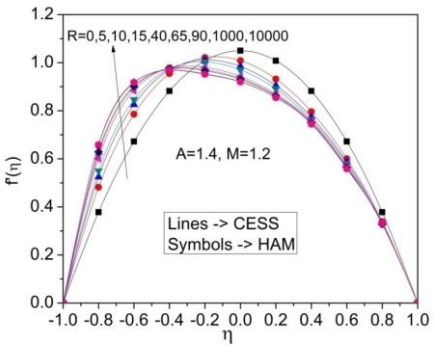


Fig.8 Variation of radial velocity for *A*=1.4, *M*=1.2 and various values of *R*.

Fig. 8 illustrates the influence of $R$ on the radial velocity profile for fixed values of $A$ and $M$. The radial velocity profile becomes symmetric for $R = 0$ with respect to the central plane z = 0 where it attains the maximum value. These profiles move towards the lower disk due to the influx velocity $V_2$ at the upper disk. It is observed that for increasing values of $R$ the radial velocity profiles decrease near the upper disk and increase near the lower disk.

The effect of the Hartmann number $M$ on the axial and radial velocity curves for fixed values of $A=1.2$ & $R=20$ are presented graphically in Figs. 9 and 10 respectively. The axial velocity profiles fall down at the upper boundary whereas small increases near the lower boundary with respect to increase in the values of $M$. The radial velocity profiles shift towards the lower disk for smaller values of $M$ and the maximum radial velocities decreases and then become flat in the middle region of the disks as $M$ increases. Further it is seen that these profiles move towards the disks as $M$ increases but a significant change is observed at the upper disk.

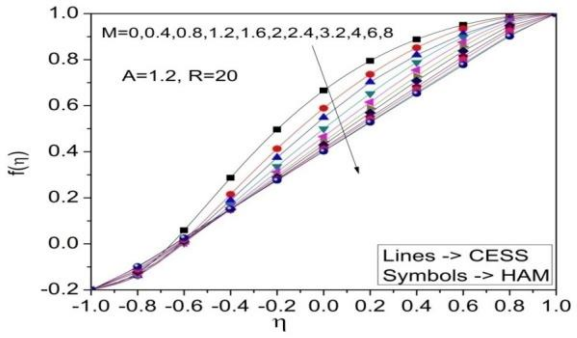


Fig.9 Variation of axial velocity for $A$=1.2, $R$=20 and various values of $M$.

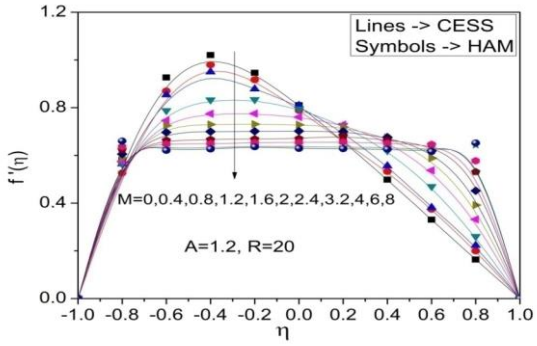


Fig.10 Variation of radial velocity for $A$=1.2, $R$=20 and various values of $M$.

Table 5 presents the convergence analysis of the HAM solutions of shear stresses for various orders of approximations. It is observed that the convergence is attained for the functions $f''(-1)$ and $f''(1)$ at 25th and 30th order of approximations respectively.

Table 5. Convergence of HAM solutions for increasing order of approximations for $A$=1.4, $M$=1.2 and $R$=10.

| Order of approximations | $f''(-1)$ | $f''(1)$ |
|---|---|---|
| 5 | 3.36665 | -1.89329 |
| 10 | 3.33022 | -1.89401 |
| 15 | 3.33221 | -1.88940 |
| 20 | 3.3325 | -1.88992 |
| 25 | 3.33242 | -1.89000 |
| 30 | 3.33242 | -1.88997 |
| 35 | 3.33242 | -1.88997 |
| 40 | 3.33242 | -1.88997 |

From all the Figures and Tables it's clear that the obtained results are in good agreement with the earlier literature work. The HAM solutions are converges fast and have good accuracy as compared to CESS results.

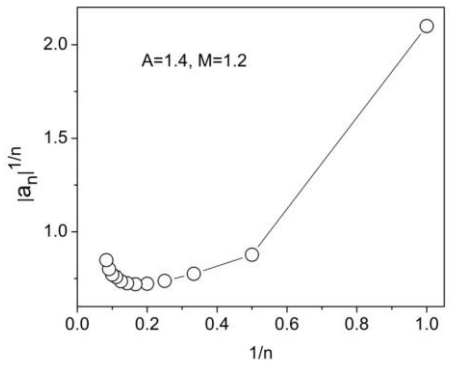


Fig.11 Domb-Sykes plot for the Eulerized series for $A$=1.4 and $M$=1.2.

## 6. Conclusion

In this paper, the analytical solutions of the boundary value problem arise in the MHD asymmetric flow between two coaxial infinite porous disks in the presence of magnetic field is discussed using CESS and HAM. The convergences of the HAM solutions are discussed through the $\hbar$ curves. From all the figures and tables it's clear that, the obtained results are in good agreement with the earlier literature work. The HAM solutions converge much faster and have good accuracy as compared to CESS results. The novel procedures presented here enables in the analysis of the series which is valid in a much larger region than the numerical methods. Shear stress values are increasing at the upper disk and are decreasing at the lower disk by increasing permeability parameter where as the reverse trends are observed for the Reynolds number.

## References:

1. M. Siddique, Imran and D. Vieru, *A new exact solution for MHD transient rotation flow of a second grade Fluid in a Porous space,* Bulletin of the Polytechnic Institute from placeCityIasi placecountry- regionROMANIA 54 (58), (2008) 27-36.
2. M. Khan, S. Hyder Ali, T. Hayat and C. Fetecau, *MHD flows of a second grade fluid between two side walls perpendicular to plate through a porous medium,* International Journal of Non-Linear Mechanics 43, (2008) 302-319.
3. T. Hayat, R. Sajjad, Z. Abbas, M. Sajid and Awatif A. Hendi, *Radiation effects on MHD flow of Maxwell fluid in a channel with porous medium,* International Journal of Heat and Mass Transfer 54, (2011) 854-862.
4. C. Fetecau, A. Mahmood, Corina Fetecau and D. Vieru, *Some exact solutions for the helical flow of a generalized Oldroyd-B fluid in circular cylinder,* Computers & Mathematics with Applications 56, (2008) 3096-3108.
5. M. Ashraf and M. M. Ashraf, *MHD stagnation point flow of a micro polar fluid towards a heated surface:* Applied Mathematics and Mechanics (English Edition) 32(1), (2011) 45-54.
6. *N. Rudraiah and B. C. Chandrasekhara,* Flow of a conducting fluid between porous disks for large suction Reynolds number,Phys *Soc. Japan 27, (1969) 1041-1045.*
7. H. Rasmussen, *Steady viscous flow between two porous disks,* Z. Angewn. Math. Phys. 21, (1970) 187-195.
8. *A. R. Elcrat,* On the radial flow of a viscous fluid between two porous disks, *Arch. Rat. Mech. Anal. 61 , (1976) 91-96.*
9. Y. N. Guar, R. C. Chaudhary, *Heat transfer for laminar flow through parallel porous disks of different permeability* placePlaceNameIndian PlaceTypeAcademy of Sciences, section A 87A, (1978) 209-217.
10. *N. Phan-Thien and M. B. Bush,* On the steady flow of a Newtonian fluid between two parallel disks, *ZAMP. 35, (1984)912-919.*
11. C. Y. Lai, K. R. Rajagopal, A. Z. Szeri, *Asymmetric flow between parallel rotating disks,* J. Fluid. Mech. 146, (1984) 203-225.

12. C. Y. Lai, K. R. Rajagopal, A. Z. Szeri, *Asymmetric flow above a rotating disk,* J. Fluid. Mech. 157, (1985) 471-492.
13. A. Singh, B. D. Vyas and U. S. Powel, *Investigations on inward flow between two stationary parallel disks,* Int. J. Heat and Fluid Flow. 20, (1999) 395-401.
14. *H. A. Attia,* On the effectiveness of the ion slip on the steady flow of a conducting fluid due to a porous rotating disk with heat transder, *Tamkang J. Sci. placecountry region Eng. 9(3), (2006) 185-193.*
15. H. V. Ersoy, *An approximate solution for flow between two disks rotating in about Distinct axes at different speeds,* Hindawi Publishing Corporation Math Problems placecountry-regionEng. 2007,1-16 (2007).
16. T. Fang and Zhang, Flow over a stretchable disk, Int. Com. Heat and mass transfer 35, (2008) 892-895.
17. *B. S. Bhatt and E. A. Hamza,* Similarity solution for the squeezed flow film between two rotating naturally permeable discs, *ZAMM. 76, (1996) 291-299.*
18. *A. R. Wehgal and M. Ashraf,* MHD asymmetric flow between two porous disks, *Journal of Mathematics. 44, (2012) 9-21.*
19. M. Van Dyke, Analysis and improvement of perturbation series, Q. J. Mech. 27(1974) 423-450.
20. V. B. Awati, N. M. Bujurke and N. N. Katagi, Computer extended series solution for the flows in a Nonparallel channels, Advances in Applied Science Research, 3(4)(2012) 2413-2423.
21. N. M. Bujurke, V. B. Awati and N. N. Katagi, Computer extended series solution for flow in a narrow channel of varying gap, Applied Mathematics and Computation, 186(2007) 54-69.
22. N. M. Bujurke, N. N. Katagi and V. B. Awati, Analysis of steady viscous flow in slender tubes, Z. angew. Math. Phys., 56 (2005) 831-851.
23. N. M. Bujurke, N. N. Katagi and V. B. Awati, Analysis of Laminar flow in a channel with one porous bounding wall, Int. Jl. Fluid Mech. Res.(IJFMR), 37(3) (2010) 1-15.
24. S. J. Liao, The proposed homotopy analysis technique for the solution of nonlinear problems, Ph.D Thesis, Shanghai Jiao Tong University. (1992)
25. Vishwanath B. Awati, Manjunath Jyoti and N. N. Katagi, Computer extended series and Homotopy analysis method for the solution of MHD flow of viscous fluid between two parallel porous plates, Gulf Journal of Mathematics, 4 (2016) 65-79.
26. M. Von Karman, *Under laminare and turbulente,* Reibung Z. Zngew Math. Mech.1, (1921) 233-235.
27. A. F. Elkouh, *Laminar flow between porous disks,* J. Eng. Mech. Div. ASCE. 93, (1967) 5375-5377.
28. C. Domb and M. F. Sykes, On the susceptibility of a ferromagnetic above the curic point, Proc. Roy. Lond. Ser. A. 240(1957) 214-228.
29. W. H. Press, S. A. Flannery, Teukolsky and W. T. Vetterling, Numerical Recipes, Cambridge University Press. (1986).
30. C. M. Bender and S. A. Orszag, Advanced Mathematical Methods for Scientists and Engineers, Third International Edition (Mc-Grawhill Book Company), (1987).